# Communication and quorum sensing in non-living mimics of eukaryotic cells

Henrike Niederholtmeyer[1], Cynthia Chaggan[1], and Neal K. Devaraj[1]*

[1]Department of Chemistry and Biochemistry, University of California, San Diego, USA.

*Correspondence to: ndevaraj@ucsd.edu

## Abstract

Cells in tissues or biofilms communicate with one another through chemical and mechanical signals to coordinate collective behaviors. Non-living cell mimics provide simplified models of natural systems, however, it has remained challenging to implement communication capabilities comparable to living cells. Here we present a porous artificial cell-mimic containing a nucleus-like DNA-hydrogel compartment that is able to express and display proteins, and communicate with neighboring cell-mimics through diffusive protein signals. We show that communication between cell-mimics allowed distribution of tasks, quorum sensing, and cellular differentiation according to local environment. Cell-mimics could be manufactured in large quantities, easily stored, chemically modified, and spatially organized into diffusively connected tissue-like arrangements, offering a means for studying communication in large ensembles of artificial cells.

## Main Text

In communities of single-celled and multicellular organisms, cell-cell communication enables cells to organize in space, distribute tasks, and to coordinate collective responses. Synthetic biologists have engineered living, communicating cells to form cellular patterns[1,2] and synchronize gene expression[3] but living systems are inherently challenging to study and engineer. Chemically constructed cell-mimics, as non-living, biochemically simplified and engineerable systems, could serve as models to study mechanisms of pattern formation and collective responses, and lead to the development of novel sensors and self-organizing materials. Important biochemical processes like protein synthesis[4,5], DNA replication[6], metabolism[7] and cytoskeletal functions[8] have been reconstituted and studied in single synthetic cell-mimics. While biochemical reactions in microfluidic chambers[9-11], in droplets[12] and on beads[13] can model aspects of intercellular communication, studies on systems that structurally resemble natural cells have focused on single, isolated cell-mimics because of limitations in assembly methods and communication channels. To address the scalable assembly of artificial cells, microfluidic methods have been developed to mass-produce phospholipid vesicles encapsulating active biomolecules[14-17]. Recent studies have demonstrated signaling between cell-mimics to induce gene expression[5,18,19] or chemical reactions[20,21] but signaling molecules have been limited to small molecules that can either freely cross membranes or require alpha-hemolysin pores. In contrast, signaling in multicellular organisms often involves secretion of proteins serving as growth factors or morphogens that provide cells with the information they need to develop into functional tissues[22].

Here, we aimed to expand the communication capabilities of artificial cells by developing a cellular mimic that produces and releases diffusive protein signals that travel in and get interpreted by large populations of cell-mimics. We describe the microfluidic production of cell-mimics with a porous polymer membrane containing an artificial hydrogel compartment, which resembles a eukaryotic cell's nucleus in that it contains the cell-mimics' genetic material for protein synthesis and can sequester transcription factors. Cell-mimics were able to communicate through diffusive protein signals, activate gene expression in neighboring cell-mimics, and display collective responses to cell-mimic density similar to bacterial quorum sensing.

## Results

We prepared porous cell-mimics capable of gene expression and communication via diffusive protein signals using a microfluidic method (**Fig. 1a, b**). First, water-in-oil-in-water double emulsion droplets were formed in a polydimethylsiloxane (PDMS) device (Fig. S1, movie 1). The droplets had a middle organic phase consisting of a 1-decanol and acrylate monomer solution and encapsulated DNA and clay minerals. Second, double emulsion droplets were collected and polymerized using UV light, inducing a phase separation of the inert 1-decanol to form porous microcapsules[23]. Third, following polymerization, we simultaneously permeabilized the polymer membrane and induced formation of a clay-hydrogel in their interior by adding a solution of ethanol and HEPES buffer. Membrane pores had diameters of 200-300 nm (**Fig. 1a**, Fig. S2). Polymer membranes were permeable to macromolecules up to 2 MDa but excluded 220 nm nanoparticles from about 90% of the microcapsules (Fig. S3). The clay hydrogel trapped DNA in the interior of the porous microcapsules (Fig. S4)[24] in a structure that is analogous to the cell nucleus (**Fig. 1c**, Fig. S5). The clay-DNA hydrogel partially excluded 2 MDa dextran but smaller macromolecules could enter (Fig. S3). Fourth, to prevent non-specific binding of proteins to the polymer membrane of cell-mimics we passivated their surface with polyethylene glycol (PEG) (Fig. S6).

The porous structure of the polymer membrane allowed supply of cell-free transcription and translation (TX-TL) reagents from the outside to induce synthesis of proteins encoded by the DNA in the cell-mimics' hydrogel nuclei. Even ribosomes, the largest components of TX-TL reagents, were able to diffuse into cell-mimics through their porous membranes (Fig. S7). To capture protein products within cell-mimics we expressed a fusion protein of the tetracycline repressor TetR and sfGFP (TetR-sfGFP) as a fluorescent reporter. TetR binds the *tet* operator sequence (*tetO*). A co-encapsulated 240x *tetO* array plasmid localized the reporter protein to the hydrogel nucleus (**Fig. 1c**), which increased in fluorescence after TX-TL addition (**Fig. 1d**, movie 2). Localization of TetR-sfGFP to the hydrogel nucleus was reversible and due to the specific interaction of TetR with *tetO* sites. Addition of anhydrotetracyline, which prevents TetR from binding DNA, caused a substantial unbinding of TetR-sfGFP. Without the *tetO* plasmid, fluorescence increased in solution but not in hydrogel nuclei (Fig. S8). In *tetR*-sfGFP / *tetO* cell-mimics, fluorescence increased substantially in almost all cell-mimics (**Fig. 1e**). Variations in intensity were likely due to differences in DNA capture during formation of hydrogel nuclei (Fig. S5). Cell-mimics retained full expression capabilities after two

years of storage, and separate batches showed comparable expression levels and dynamics (Fig. S9).

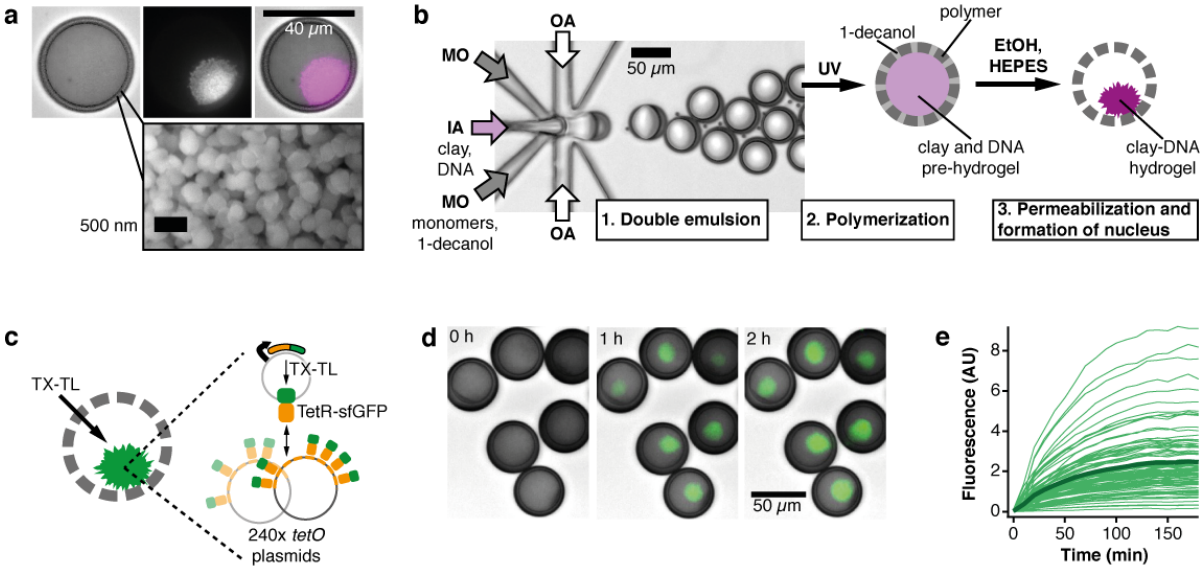


**Fig. 1. Formation of cell-mimics containing artificial "nuclei" capable of gene expression.**
**a)** Optical micrographs (top) of a cell-mimic with GelRed stained hydrogel "nucleus" (brightfield, red fluorescence, merge) and scanning electron microscopy of porous cell-mimic membrane (bottom). **b)** Microfluidic production of double emulsion droplets encapsulating a pre-hydrogel in a photocurable middle layer, and schematic of subsequent processing steps. IA: Inner aqueous, MO: middle organic, OA: Outer aqueous phase. **c)** Schematic and timelapse images **(d)** of expression and capture of TetR-sfGFP in hydrogel nuclei (green, merged with brightfield images). TX-TL reagents were added at 0 h. **e)** Dynamics of fluorescence signal increase in the hydrogel nuclei of 100 cell-mimics with average shown in bold.

Due to their porosity, cell-mimics likely released mRNA and protein products that diffused into neighboring cell-mimics. To demonstrate that neighboring cell-mimics exchanged protein products with each other, we prepared "sender" cell-mimics, fluorescently labeled in their polymeric membranes and containing the *tetR*-sfGFP expression plasmid, and "receiver" cell-mimics containing the *tetO* array plasmid to capture the reporter protein. When both cell-mimic types were mixed at approximately a one to one ratio, only the nuclei of the receiver cell-mimics increased in fluorescence (**Fig. 2a**). To explore how far TetR-sfGFP protein originating from a given sender cell-mimic travelled, we used a large excess of receivers and spread them densely into a circular 3.5 mm wide "colony". Under these conditions, TetR-sfGFP spread from sender to surrounding receiver cell-mimics but stayed localized in patches around individual sender cell-mimics (**Fig 2b**, Fig. S10a). This pattern of captured protein around source cell-mimics persisted for 24 h after expression ended, demonstrating that TetR-sfGFP was essentially trapped in the hydrogel nuclei once it was bound in the high local density of *tetO* sites. Assuming free diffusion, we would expect protein gradients to have disappeared within 5 h in similar geometries (Fig. S10b-d).

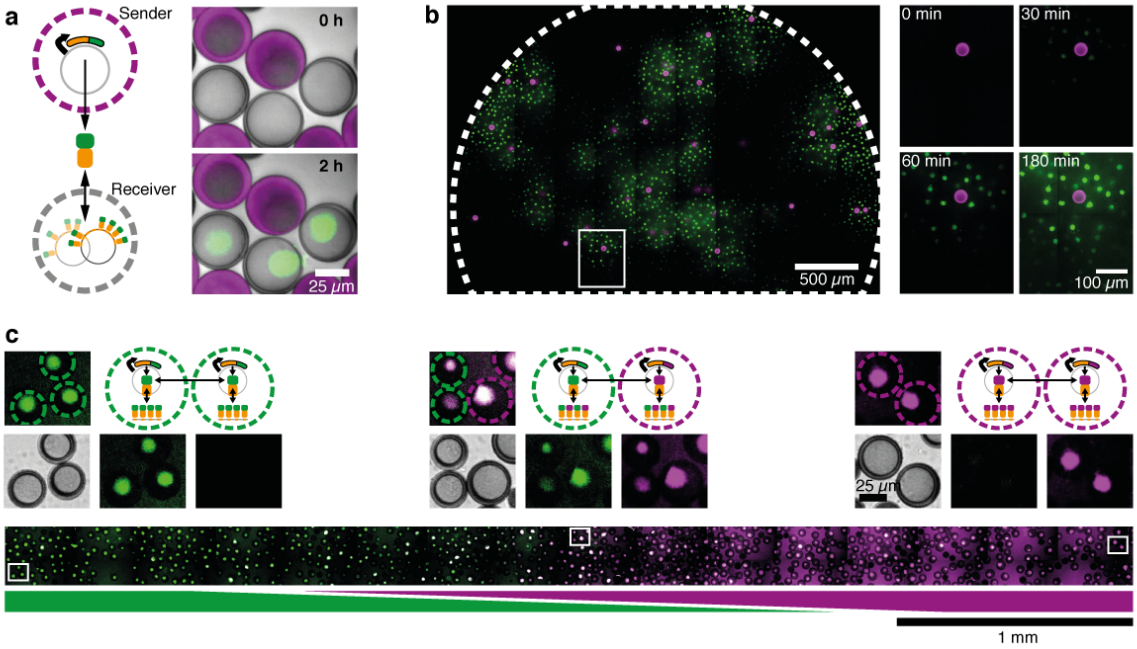


**Fig. 2. Protein exchange between neighboring and distant cell-mimics.**
**a)** Schematic of diffusive TetR-sfGFP exchange between neighboring sender and receiver cell-mimics and timelapse images of neighboring senders (rhodamine B stained membranes) and receivers (unstained membranes). Merge of brightfield and fluorescence channels (sender membranes, magenta; TetR-sfGFP, green).
**b)** Distribution of TetR-sfGFP (green) in a dense droplet of receivers and sparse senders (magenta) after 3 h of expression. A small region around a sender (white box) is magnified and spreading of fluorescence is shown at different time points.
**c)** Inhomogeneous mix of two types of cell-mimics producing and binding different color reporter proteins. *tetR*-sfGFP / *tetO* (green) and *tetR*-mCherry / *tetO* cell-mimics (magenta) were distributed in a channel to stay separate at the sides and mix in the center. Bottom image shows the distribution of sfGFP and mCherry fluorescence after 5 h. Merge of the two channels results in a white signal (middle). Magnified images from indicated positions along the channel are shown above. Merged image with cell-mimic types indicated by colored, dashed circles (top), and brightfield, sfGFP and mCherry signals shown separately (below).

To test the preference of a given cell-mimic to bind protein originating from its own DNA, we prepared *tetR*-mCherry / *tetO* cell-mimics that accumulated red fluorescence in their hydrogel nuclei (Fig. S10). When mixed with *tetR*-sfGFP / *tetO* cell-mimics (**Fig. 1c**), there was essentially no difference in relative fluorescence in either channel between the cell-mimic types, indicating that in close proximity, neighboring cell-mimics completely exchanged protein products (Fig. S11). While transcription occurred in the hydrogel nuclei where DNA was localized, these results indicate that translation was likely not localized to the cell-mimic a given mRNA originated from. However, because mRNA lifetime in TX-TL reagents is short, and mRNA thus has a limited diffusion range, we expected the localization of TetR-sfGFP and TetR-mCherry to depend strongly on distance between cell-mimics. We distributed the two cell-mimic types in a reaction

chamber so that they mixed in the center but remained separate on either side. Cell-mimics in the center showed mixed fluorescence while cell-mimics on the sides fluoresced primarily in one channel (**Fig. 2c**), demonstrating that locally, on the order of few cell-mimic lengths, proteins exchanged with little hindrance by the polymer membranes, whereas exchange of protein with distant cell-mimics was limited by diffusion.

Communication in vesicle-based cell-mimics has so far been limited to small molecule signals such as quorum sensing molecules[18,19] or IPTG and glucose, combined with membrane pores, like alpha-hemolysin[5,21]. Our porous cell-mimics exchanged proteins with their neighbors, suggesting they are able to communicate with each other directly through genetic regulators. To demonstrate this we constructed a two-stage activation cascade and distributed the network into two separate cell-mimic types. T3 RNA polymerase (T3 RNAP) served as a diffusive signaling molecule transmitting the instruction to express a reporter gene from "activator" to "reporter" cell-mimics. Activator cell-mimics contained the template for the expression of T3 RNAP. Reporter cell-mimics contained the template for the T3 RNAP-driven synthesis of the TetR-sfGFP reporter as well as *tetO* array plasmids to capture the reporter protein. When both cell-mimic types were mixed, reporter cell-mimics expressed and bound the fluorescent reporter (**Fig. 3**, movie 3), while activator cell-mimics alone did not increase in fluorescence (Fig. S12).

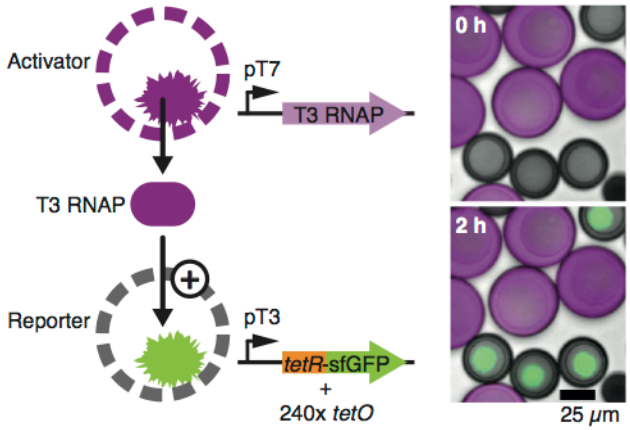


**Fig. 3. Communication between cell-mimics via a diffusive genetic activator.** Schematic of the two types of cell-mimics communicating through a distributed genetic activation cascade. Micrographs show a merge of brightfield images with rhodamine B fluorescence in the membranes of activators (magenta) and fluorescence of TetR-sfGFP (green) in the hydrogel nuclei of reporters directly after addition of TX-TL and after 2 h of expression.

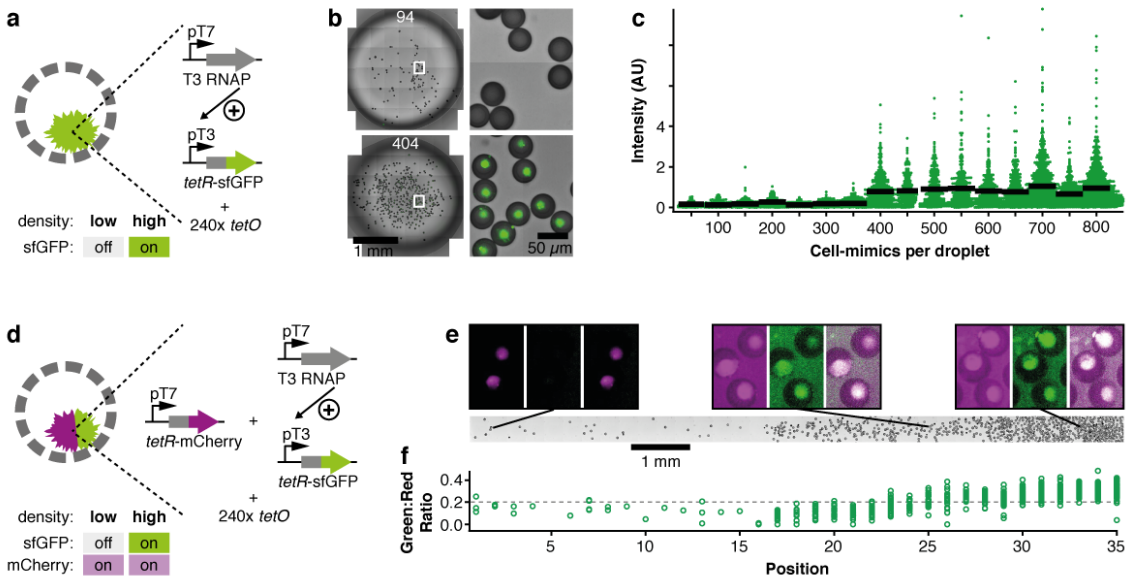


**Fig. 4. Density sensing in populations of cell-mimics.**
**a)** Artificial quorum sensing cell-mimics contain T3 activation cascade DNA templates and 240x *tetO* plasmids. **b)** Micrographs of cell-mimics in 4.5 µl droplets of TX-TL (left). The number of cell-mimics is indicated. Enlarged regions (indicated by white boxes) show presence and absence of fluorescence (green) in hydrogel nuclei after 3 h of expression. **c)** Scatter dot plot of fluorescence intensities in individual cell-mimics at different densities. Each density category combines data in increments of 50 cell-mimics per droplet and contains data from at least 156 cell-mimics (Methods). Black bars show average fluorescence. **d)** A 2-color response to density is achieved by adding a constitutively expressed reporter (pT7-*tetR*-mCherry), which is "on" independent of density. **e)** 2-color density sensors were spread at increasing density in an elongated chamber (brightfield image, bottom). Panels above show magnified fluorescence images of indicated regions (mCherry fluorescence: magenta, left; sfGFP fluorescence: green, middle; merge of fluorescence channels: right). Images in each channel are window leveled to the same values and have a width of 70 µm. **f)** Ratio between sfGFP to mCherry fluorescence in individual hydrogel nuclei along the chamber. Positions correspond to tile regions of the image above.

We hypothesized that T3 RNAP could serve as a soluble signaling molecule providing cell-mimics with information about population density. Indeed, cell-mimics containing both the activation circuit and reporter constructs (**Fig. 4a**) underwent a collective response where fluorescence accumulated in cell-mimics only at high densities. At low cell-mimic densities, signals from the hydrogel nuclei were not detectably different from background fluorescence (**Fig. 4b**). We titrated the density of cell-mimics in a fixed volume and found a sharp transition from "off" to "on," which resembled bacterial quorum sensing responses to cell density[25]. The threshold cell-mimic density at which expression of the reporter turned on was 400 cell-mimics in 4.5 $\mu$l TX-TL (**Fig. 4c**). Cell-mimics that constitutively expressed the reporter (**Fig. 1c**) accumulated fluorescence in their hydrogel nuclei regardless of their density (Fig. S13). The collective response to density can be explained by T3 RNAP release from cell-mimics. At low densities, T3

RNAP is diluted in the comparably large volume of the sample, while at high density a sufficient concentration of transcriptional activator accumulates to turn on expression of the reporter. Titrating the T3 RNAP template DNA in TX-TL reactions, we found a similarly sharp transition in expression with a half-maximal activation at 10 pM (Fig. S14). The calculated bulk concentration of T3 RNAP template in an artificial quorum sensing experiment at the threshold density of 400 cell-mimics per droplet is 12.5 pM, similar to the activation threshold in bulk solution.

During development, cells interpret signals secreted by their neighbors to differentiate into specialized cell-types that express different sets of genes[22]. We aimed to mimic cellular differentiation according to local environment by combining the artificial quorum sensing network with a constitutively expressed *tetR*-mCherry reporter that turns on irrespective of cell-mimic density (**Fig. 4d**). We distributed cell-mimics unevenly in a long narrow reaction chamber (**Fig. 4e**), and analyzed the fluorescence of individual hydrogel nuclei according to their location in the density gradient. While absolute fluorescence intensities and background fluorescence increased with cell-mimic density, hydrogel nuclei from the high density area displayed visibly higher sfGFP:mCherry ratios than hydrogel nuclei in the dilute region that primarily displayed mCherry fluorescence (**Fig. 4f**). In the continuous density gradient we observed some graded responses in the center of the chamber at medium density. However, plotting sfGFP against mCherry fluorescence for individual hydrogel nuclei revealed two distinct populations of fluorescence signals according to position in the chamber (Fig. S15).

**Discussion**

We developed porous cell-mimics capable of gene expression and communication via diffusive protein signals. The clay-DNA hydrogel in the cell-mimic's interior resembles a eukaryotic cell's nucleus, and represents a novel way to compartmentalize artificial cells[16,26,27]. Clay minerals have been proposed as favorable environments for prebiotic evolution because a wide variety of organic molecules adsorbs to their surface and because of their catalytic properties[28]. Our and a previous study[24] demonstrate the useful properties of Laponite clay hydrogels for cell-free synthetic biology and for the assembly of artificial cell-mimics as hybrids of organic and inorganic materials. Unlike lipid vesicles that require careful matching of osmolarities and gentle separation techniques, the cell-mimics reported here with their porous polymer membranes were physically highly stable, easily transferred into new media by centrifugation, and retained full expression capabilities after two years of storage. Microfluidic production of highly homogeneous cell-mimics will facilitate studies requiring large quantities of cell-mimics as our results on spatially arrayed, communicating cell-mimics demonstrate. Passivating cell-mimics' polymer membranes with PEG, we showed that their membranes could be chemically modified, which will allow further functionalization, for example for immobilization on substrates, to target specific proteins to the membrane or to tune membrane permeability.

So far, communication in synthetic, non-living cell-mimics has been limited to small molecule signals[5,18-21]. The porous cell-mimics developed here expand the communication capabilities of artificial cells to large macromolecules like RNAs and proteins. We

showed that genetic circuits could be distributed into separate cell-mimics, which allowed them to share tasks. Such modularity might facilitate prototyping of gene circuits by titrating cell-mimics containing different parts of a network. Furthermore, individual components of circuits located in different cell-mimics can be spatially organized to generate spatiotemporal expression patterns. Protein signals play an important role for cell-cell communication in multicellular organisms, where cells release and receive protein signals in the form of hormones, growth factors and morphogens[22]. We anticipate that developmental processes in multicellular organisms can be modeled in artificial, tissue-like arrangements of cell-mimics. Clearly, a major difference between an artificial tissue assembled from porous cell-mimics and natural tissues is that translation of proteins takes place both inside and outside of the cell-mimic a given mRNA originates from, and that mRNAs and proteins can freely diffuse. In this regard, our system models features of the syncytium stage during *Drosophila* embryogenesis, when thousands of nuclei accumulate in the unseparated cytoplasm of the oocyte[29]. In another analogy to this developmental stage we showed trapping of the TetR transcription factor in nuclei containing its binding sites. Nuclear trapping is a mechanism that is responsible for establishing sharp gradients of phosphorylated ERK/MAPK (dpERK) across the syncytical *Drosophila* embryo by limiting diffusion of dpERK[30].

A genetic activation circuit led to a remarkable collective response to cell-mimic density, which resembled bacterial quorum sensing. In contrast to bacterial quorum sensing[25], the mechanism of our artificial quorum sensing involved no positive feedback loop and employed a protein instead of a small molecule, showing that artificial cells can model biological phenomena using unnatural parts and mechanisms. Collective responses can lead to greater accuracy and reduce noise[3], which will be particularly helpful for the assembly of reliably functioning cell-mimics, which often suffer from variability in gene expression[5,31].

In conclusion, our system has a number of potential uses, including programming cell-mimics to collectively sense and respond to their environment. Indeed, artificial cell-mimics could be used to develop sensors and self-organizing materials, as well as being arrayed into synthetic tissues of artificial cells, which could serve as simplified models for reaction-diffusion processes.

## Methods

*Fabrication of microfluidic chips*

PDMS devices were prepared by standard soft lithography methods to produce devices with a design as shown in Fig. S1 and a channel height of 43 μm. Bonding and surface treatment was performed as described[15] (see Supplementary Information).

*Production of porous cell-mimics with clay-DNA hydrogel nuclei*

2 % (wt/vol) Laponite XLG (BYK Additives) clay stock was prepared by mixing 10 ml of ultrapure $H_2O$ on a magnetic stir plate to create a vortex. 200 mg of Laponite XLG were slowly added into the vortex and left to stir for 2 h until clear. The dispersion was then stored at 4°C and used for up to a week. Photoinitiator 2,2-Dimethoxy-2-

phenylacetophenone was dissolved at 5 % (wt/vol) in 1-decanol and in Trimethylolpropane ethoxylate triacrylate (ETPTA, Sigma-Aldrich, Mn 428). ETPTA with photoinitiator was stored at 4°C and used for up to a week. Double emulsion droplets were prepared with an inner aqueous solution (IA) containing 0.4 % (wt/vol) laponite XLG, 15 % (vol/vol) glycerol, 50 mg/ml poloxamer 188, 20 µM sulfo-Cy5 and up to 300 ng/µl plasmid or linear DNA. The middle organic phase (MO) was composed of glycidyl methacrylate (GMA, Sigma-Aldrich), ETPTA, and 1-decanol at a 48:32:20 ratio and contained 2.6 % (wt/vol) photoinitiator and 0.25 % (vol/vol) Span-80 to produce porous microcapsules[23]. For fluorescently labeled microcapsule membranes, the MO phase contained 0.1 mg/ml Methacryloxyethyl thiocarbamoyl rhodamine B. The outer aqueous phase (OA) was 15 % (vol/vol) glycerol with 50 mg/ml poloxamer 188. Using syringe pumps, the three phases were flowed through the microfluidic device at speeds of 3 to 12 µl/hr for the IA, 30 to 70 µl/hr for the MO and 250 to 500 µl/hr for the OA phase. Flow rates were adjusted to produce a stable formation of double emulsion droplets and then left unchanged for collection of droplets. Typically, about 200 µl of double emulsion were collected from the chip. The emulsion was then placed in a 2mm thick chamber built from cover glass and exposed to 350 nm UV light for 30 seconds using a UV reactor (Rayonet). The dispersion of polymerized microcapsules was then added to 2 ml solution of 70 % Ethanol containing 200 mM HEPES pH 8 to permeabilize the shell and to form the DNA-clay hydrogel nucleus. This stock was stored at -20°C until use.

To prevent non-specific binding of proteins to porous polymer membranes, microcapsules were treated with polyethylene glycol (PEG). We coupled amino-PEG12-alcohol to the epoxide functionalities on the polymer shells. First, microcapsules were washed with 200 mM sodium carbonate buffer pH 10 by centrifugation. All supernatant was removed from the capsule pellet and a solution of 250mM amino-PEG12-alcohol in 50% ethanol pH 10 was added to the pellet. Microcapsules were incubated at 37°C for reaction overnight and then washed with 100 mM HEPES pH 8. These PEGylated cell-mimics were either used directly or stored in 70 % ethanol 200 mM HEPES pH 8 at -20°C.

*Gene expression in cell-mimics*

For cell-mimics, expression reactions typically consisted of 1 µl concentrated cell-mimics in 100 mM HEPES pH 8 and TX-TL reagents[32] (for preparation see Supplementary Information) for a final volume of 5 µl. Droplets of 4.5 µl of this mixture were pipetted onto a 35 mm Lumox dish (Sarstedt). The gas permeable substrate ensured homogeneous sfGFP expression in the sample. The cell-mimic droplet was covered with cover glass and sealed with a ring of vacuum grease to prevent evaporation and provide a spacer. The reaction volume was scaled up for experiments in larger samples, and was 20 µl in Fig. 2b and 35 µl for long, narrow reaction chambers in Fig. 2c and Fig. 4e. Long, narrow reaction chambers were made from two parallel 20 mm lines of vacuum grease with a gap of 2 mm, which was filled with TX-TL and cell-mimics and then sealed with cover glass.

*Imaging and image analysis*

Images were acquired using a spinning disk confocal microscope consisting of a Yokagawa spinning disk system (Yokagawa, Japan) built around an Axio Observer Z1

motorized inverted microscope (Carl Zeiss Microscopy GmbH, Germany) with a 20x 1.42 NA objective. Large regions were imaged as tiles and stitched using ZEN Blue software. Further image processing and analyses were performed as described in the Supplementary Information.

**References:**


1. Basu, S., Gerchman, Y., Collins, C. H., Arnold, F. H. & Weiss, R. A synthetic multicellular system for programmed pattern formation. *Nature* **434,** 1130–1134 (2005).
2. Morsut, L. *et al*. Engineering Customized Cell Sensing and Response Behaviors Using Synthetic Notch Receptors. *Cell* **164,** 780–791 (2016).
3. Danino, T., Mondragón-Palomino, O., Tsimring, L. & Hasty, J. A synchronized quorum of genetic clocks. *Nature* **463,** 326–330 (2010).
4. Noireaux, V. & Libchaber, A. A vesicle bioreactor as a step toward an artificial cell assembly. *Proceedings of the National Academy of Sciences* **101,** 17669–17674 (2004).
5. Adamala, K. P., Martin-Alarcon, D. A., Guthrie-Honea, K. R. & Boyden, E. S. Engineering genetic circuit interactions within and between synthetic minimal cells. *Nature Chemistry* **9,** 431–439 (2017).
6. van Nies, P. *et al*. Self-replication of DNA by its encoded proteins in liposome-based synthetic cells. *Nature Communications* 1–12 (2018). doi:10.1038/s41467-018-03926-1
7. Lee, K. Y. *et al*. Photosynthetic artificial organelles sustain and control ATP-dependent reactions in a protocellular system. *Nat Biotechnol* **36,** 530–535 (2018).
8. Keber, F. C. *et al*. Topology and dynamics of active nematic vesicles. *Science* **345,** 1135–1139 (2014).
9. Tayar, A. M., Karzbrun, E., Noireaux, V. & Bar-Ziv, R. H. Propagating gene expression fronts in a one-dimensional coupled system of artificial cells. *Nat Phys* 1037–1041 (2015). doi:10.1038/nphys3469
10. Tayar, A. M., Karzbrun, E., Noireaux, V. & Bar-Ziv, R. H. Synchrony and pattern formation of coupled genetic oscillators on a chip of artificial cells. *Proc Natl Acad Sci USA* **114,** 11609–11614 (2017).
11. Zadorin, A. S. *et al*. Synthesis and materialization of a reaction-diffusion French flag pattern. *Nature Chemistry* **9,** 990–996 (2017).
12. Villar, G., Graham, A. D. & Bayley, H. A tissue-like printed material. *Science* **340,** 48–52 (2013).
13. Gines, G. *et al*. Microscopic agents programmed by DNA circuits. *Nature Nanotechnology* **12,** 351–359 (2017).
14. van Swaay, D. & deMello, A. Microfluidic methods for forming liposomes. *Lab*

*Chip* **13,** 752 (2013).

15. Deshpande, S., Caspi, Y., Meijering, A. E. C. & Dekker, C. Octanol-assisted liposome assembly on chip. *Nature Communications* **7,** 10447 (2016).
16. Deng, N.-N., Yelleswarapu, M., Zheng, L. & Huck, W. T. S. Microfluidic Assembly of Monodisperse Vesosomes as Artificial Cell Models. *J Am Chem Soc* **139,** 587–590 (2017).
17. Stachowiak, J. C., Richmond, D. L., Li, T. H., Brochard-Wyart, F. & Fletcher, D. A. Inkjet formation of unilamellar lipid vesicles for cell-like encapsulation. *Lab Chip* **9,** 2003–8 (2009).
18. Lentini, R. *et al*. Two-Way Chemical Communication between Artificial and Natural Cells. *ACS Cent. Sci.* **3,** 117–123 (2017).
19. Rampioni, G. *et al*. Synthetic cells produce a quorum sensing chemical signal perceived by Pseudomonas aeruginosa. *Chem. Commun. (Camb.)* **54,** 2090–2093 (2018).
20. Sun, S. *et al*. Chemical Signaling and Functional Activation in Colloidosome-Based Protocells. *Small* **12,** 1920–1927 (2016).
21. Tang, T. Y. D. *et al*. Gene-Mediated Chemical Communication in Synthetic Protocell Communities. *ACS Synth. Biol.* **7,** 339–346 (2018).
22. Basson, M. A. Signaling in Cell Differentiation and Morphogenesis. *Cold Spring Harbor Perspectives in Biology* **4,** a008151–a008151 (2012).
23. Kim, B., Jeon, T. Y., Oh, Y.-K. & Kim, S.-H. Microfluidic Production of Semipermeable Microcapsules by Polymerization-Induced Phase Separation. *Langmuir* **31,** 6027–6034 (2015).
24. Yang, D. *et al*. Enhanced transcription and translation in clay hydrogel and implications for early life evolution. *Sci Rep* **3,** 3165 (2013).
25. Ng, W.-L. & Bassler, B. L. Bacterial Quorum-Sensing Network Architectures. *Annu. Rev. Genet.* **43,** 197–222 (2009).
26. Peters, R. J. R. W. *et al*. Cascade Reactions in Multicompartmentalized Polymersomes. *Angew. Chem. Int. Ed.* **53,** 146–150 (2013).
27. Deng, N.-N. & Huck, W. T. S. Microfluidic Formation of Monodisperse Coacervate Organelles in Liposomes. *Angew. Chem. Int. Ed.* **56,** 9736–9740 (2017).
28. Hanczyc, M. M., Fujikawa, S. M. & Szostak, J. W. Experimental models of primitive cellular compartments: encapsulation, growth, and division. *Science* **302,** 618–622 (2003).
29. Johnston, D. S. & Nüsslein-Volhard, C. The origin of pattern and polarity in the Drosophila embryo. *Cell* **68,** 201–219 (1992).
30. Coppey, M., Boettiger, A. N., Berezhkovskii, A. M. & Shvartsman, S. Y. Nuclear Trapping Shapes the Terminal Gradient in the Drosophila Embryo. *Current Biology* **18,** 915–919 (2008).

31. Caschera, F. & Noireaux, V. Compartmentalization of an all- E. coliCell-Free Expression System for the Construction of a Minimal Cell. *Artificial Life* 1–11 (2016). doi:10.1162/ARTL_a_00198

32. Didovyk, A., Tonooka, T., Tsimring, L. & Hasty, J. Rapid and Scalable Preparation of Bacterial Lysates for Cell-Free Gene Expression. *ACS Synth. Biol.* **6,** 2198–2208 (2017).

**Acknowledgements**
This work was supported by the Department of Defense (Army Research Office) through the Multidisciplinary University Research Initiative (MURI), award W911NF-13-1-0383. H. N. was supported by a Swiss National Science Foundation fellowship. We thank Lev Tsimring, Partho Ghosh and Andrew Rudd for helpful comments on the manuscript, Ahanjit Bhattacharya for labeled ribosomes, Andriy Didovyk for *E. coli* strain BL21-Gold (DE3)/pAD-LyseR, and Prof. Jeff Hasty and Ryan Johnson for their collaboration in microfluidic chip fabrication. We thank the UCSD School of Medicine Microscopy Core with grant NS047101 and Jennifer Santini for assistance with scanning electron microscopy, and the Waitt Advanced Biophotonics Core Facility of the Salk Institute with funding from NIH-NCI CCSG: P30 014195, NINDS Neuroscience Core Grant: NS072031 and the Waitt Foundation.

**Author contributions**
H.N. and N.K.D. conceived the study and designed experiments. H.N. and C.C. performed experiments. H.N. analyzed the data. H.N. and N.K.D wrote the manuscript. All authors read and accepted the manuscript.

**Competing financial interests**
The authors declare no competing financial interests.

**Supplementary Information**
Supplementary Methods
Figs. S1 – S15
Tables S1 – S2
Movies S1 – S3